Modulator Effect in UiO-66-NDC (1,4-Naphthalenedicarboxylic Acid) Synthesis and Comparison with UiO-67-NDC Isoreticular Metal–Organic Frameworks

Butova, V. V.; Budnyk, A. P.; Guda, A. A.; Lomachenko, K. A.; Bugaev, A. L.; Soldatov, A. V.; Chavan, S. M.; Oien-Odegaard, S.; Olsbye, U.; Lillerud, K. P.; Atzori, C.; Bordiga, S.; Lamberti, C.

Modulator Effect in UiO-66-NDC (1,4-Naphthalenedicarboxylic Acid) Synthesis and Comparison with UiO-67-NDC Isoreticular Metal-Organic Frameworks.

Cryst. Growth Des. **2017,** *17*, 5422-5431

Doi: 10.1021/acs.cgd.7b00892

Modulator effect in UiO-66-NDC (1,4-naphthalenedicarboxilic acid) synthesis and comparison with UiO-67-NDC isoreticular MOFs

Vera V. Butova[a,*], Andriy P. Budnyk[a], Alexander A. Guda[a], Kirill A. Lomachenko[a,b], Aram L. Bugaev[a,c], Alexander V. Soldatov[a], Sachin M. Chavan[d], Sigurd Øien-Ødegaard[d], Unni Olsbye[d], Karl Petter Lillerud[d], Cesare Atzori[c], Silvia Bordiga,[c,d] Carlo Lamberti[a,e,*]

[a] *International research center "Smart Materials", Southern Federal University, 5 Zorge str., Rostov-on-Don, 344090, Russia.*
[b] *European Synchrotron Radiation Facility, Grenoble Cedex 9, 38043 France.*
[c] *Department of Chemistry, NIS Interdepartmental Center, INSTM Reference center, University of Turin, Via P. Quarello 15, I-10135 Turin, Italy.*
[d] *Department of Chemistry, University of Oslo, N-0371 Oslo, Norway*
[e] *Department of Chemistry, CrisDi Interdepartmental Center, INSTM Reference center, University of Turin, Via P. Giuria 7, I-10125 Turin, Italy.*

Abstract
A zirconium metal organic framework with UiO-66 topology was synthesized using 1,4-naphthalenedicarboxylic acid linker (UiO-66-NDC). From synchrotron XRPD we found that the naphthalene rings of the NDC linker is out of (*a*,*c*)-plane equilibrium by 30 °, similar to the situation found by single crystal XRD for the benzene rings in UiO-67 [*Cryst. Growth Des*. **2014**, *14*, 5370]. Different fraction of benzene-carboxylic (BC) acid modulator vs. NDC were used to tune structural properties of the final product. Modulator increases both the crystal size and the surface area of the product, but reduces its thermal stability owing to insertion of defects: missing linkers and missing $Zr_6(OH)_4O_4$ clusters. This study proves that the defect density (fraction of BC incorporation) can be tuned in UiO-66-NDC materials up to almost 50 %. At that stage, the crystal is characterized also by high density of missing $Zr_6(OH)_4O_4$ inorganic cornerstones. Notwithstanding such structural defectivity, even the most defective material is stable after thermal activation at 200 °C (able to fully remove the solvent) and in water conditions, opening possibilities for application in the fields of catalysis and molecule sorption.

1. Introduction.

Metal-organic frameworks (MOFs)[1-2] are a new class of porous materials with high surface area attracting attention due to their numerous potential applications for selective gas absorption[3] and storage,[4-6] catalysis,[7-11] biomedicine,[12-13] and others.[14-18] One of the major reason for their success in so many fields is the high flexibility in their structure and composition as they consist of metal-oxygen clusters (or secondary building units, SBUs) connected by organic molecules (linkers). In 2008 (and successive works), Lillerud group reported a new family of zirconium-based MOF, namely, UiO-66,67,68 (UiO stands for University of Oslo) with unprecedented thermal, chemical and mechanical stability,[19-31] that have found a wide range of applications.[32-36] The prototype member of this family is UiO-66, with 1,4-benzene-dicarboxylate (BDC) as a linker and $Zr_6O_4(OH)_4$ as the SBU, that transforms into Zr_6O_6 upon solvent removal.[21-23] It has even been foreseen that the all-gas-phase synthesis of UiO-66 through modulated atomic layer deposition could enable implementations in microelectronics.[34] The framework is preserved up to 400 °C in air and possess a high surface area of 1236 m^2/g.[37] In 2014 Shearer *et al.* reported that various synthesis methods can be used to tune the BDC incorporation in the framework, influencing both the surface area and the thermal stability of UiO-66.[24]

In 2009 the "coordination modulator" concept was introduced by Tsuruoka *et al.* for capping reagents, who used carboxylic acids to regulate the rate of framework extension and crystal growth.[38] Later on, other groups reported that addition of modulators to the synthesis of HKUST-1 results in formation of bigger crystals.[39-40] Similar approach was further adopted for synthesis of UiO-66-type MOFs, reaching higher surface area and better catalytic activity with respect to unmodulated UiO-66.[41-42] Schaate *et al.*[43] employed benzoic and acetic acids as modulators for synthesis of UiO-66 and other UiO-type structures.

The control of the defect chemistry in MOFs, in particular for UiO-66, has been investigated in order to achieve better performances in many applications. This approach has been named "defect engineering" as a shorthand for the ability to manipulate defects by a synthetic and controlled way. Many authors recently shown with their works several fascinating ways to achieve this kind of defect control.[16, 24, 29, 31-32, 35, 37, 42, 44-49]

On the other hand, Garibay *et al.*,[50] following a slightly modified procedure from Ref.,[19] obtained a MOF with UiO-66 topology replacing BDC linkers with 1,4-naphthalenedicarboxylic acid (1,4-NDC). Due to structural similarity, it is labelled hereafter as UiO-66-NDC. The replacement of the linker opens new possibilities such as an increased affinity towards post-synthesis π-functionalization on the naphthalene rings.[20] Starting reagents were $ZrCl_4$, 1,4-NDC and N,N-dimethylformamide (DMF) with molar ratio 1:1:143. No modulator was used in that synthesis.[50] Similarly, Huang *et al.*[51] employed 2,5-dimethylterephthalic acid (2,5-BDC-$(CH_3)_2$) in order to synthesize UiO-66-$(CH_3)_2$, a material that shown enhanced chemical stability towards water adsorption and an improved performance in CO_2 adsorption in respect to the plain UiO-66.

In the present work, we further modified the synthesis technique and investigated how benzene-carboxylic (BC) acid, acting as modulator, affects UiO-66-NDC properties. For the first time, we refined the influence of the BC/NDC ratio on the formation of UiO-66-NDC phase (vide infra Table **1**).

2. Experimental and methods.

2.1 MOF synthesis

The chemicals $ZrCl_4$, 1,4-NDC, BC acid, DMF were purchased from Alfa Aesar and used without further purification. Deionized (DI) water (18 MΩ cm) was obtained from Simplicity UV ultra-pure water system. In a typical procedure, $ZrCl_4$ (0.250 g) was dissolved in 25 ml of DMF in a conical flask, and 57.9 µl of DI water was added. Then, a respective amount of BC, as reported in

Table 1. Molar composition of the reagents and average size (<L>) of the resulting UiO-66-NDC crystals after 24 h of synthesis. Comparable results have been obtained for the 96 h synthesis. Also reported in the last four columns are the surface area and the pore volume obtained from N_2 adsorption isotherms applying both BET and Langmuir methods (vide infra Section 3.2). Pore volumes were calculated at $P/P_0 = 0.5$ and taking into account the density of liquid N_2 at 77 K.[52-53] NP = no precipitate.

Sample	$ZrCl_4$	1,4NDC	H_2O	BC	DMF	<L>	Surface Area ($m^2\ g^{-1}$)		Pore Volume
name	mol	mol	mol	mol	mol	nm	BET	Langmuir	($mm^3\ g^{-1}$)
0BC	1	1	3	0	300	80	448	593	221
10BC	1	1	3	10	300	150	575	696	260
60BC	1	1	3	60	300	800	693	840	319
100BC	1	1	3	100	300	NP	–	–	–

Table **1**, was poured into the flask with $ZrCl_4$ solution, and 1,4-NDC (0.232 g) was added. After complete dissolution of the reagents, the flask was sealed and placed into the preheated oven at 120 °C for 24 h. In this way, we obtained three samples labelled in respect to added amount of BC: 0BC (without BC acid), 10BC and 60BC with 10 and 60 equivalents of BC acid, respectively (

Table **1**). The synthesis performed using 100 equivalents of BC resulted in no precipitate even after 96 h at 120 °C. Also for the other molar compositions (0BC, 10BC and 60BC) the synthesis was duplicated increasing the heating time at 120 °C to 96 h. In those cases, there was no significant difference in the XRD profiles and in the product yield, indicating that 24 h is sufficient to complete the synthesis. For comparison, a standard UiO-66 was obtained in the same conditions using BDC as a linker but without BC modulator.

2.2. Characterization techniques

Diffraction patterns were measured in 0.7 mm rotating glass capillaries at the European Synchrotron Radiation Facility (ESRF), beamline BM01B[54] (successively moved to BM31) for 0BC, 10BC and 60BC samples, and for the standard UiO-66 for comparison. Twenty diffraction patterns were measured for each sample with a CMOS-Dexela 2D detector and averaged before the analysis. Wavelength of the incoming beam, λ = 0.505235(5) Å, and sample-to-detector distance were calibrated using LaB_6 and silicon powder standards. The adopted experimental set-up allowed us to cover the 1.4–40.0 ° 2θ range, which corresponds to the Q-range from 0.30 to 8.51 $Å^{-1}$ and to a *d*-spacing ranging from 20.68 down to 0.74 Å. Subsequent averaging and integration were carried out using the PyFAI software.[55] Profile analysis was performed using Jana2006 software.[56] Framework stability of 0BC-60BC series was further checked by laboratory XRPD collected in the 30-500 °C temperature interval, with an X-ray powder diffraction system ARL X'TRA (Thermo Scientific) using Cu-K_α radiation.

Ultra-high resolution Scanning Electron Microscope of Hitachi SU8230 type was used to obtain high resolution images of the material. The sample was mounted on a carbon tape prior to the measurement. The surface area and porosity were determined by BET and Langmuir methods from nitrogen physisorption isotherms obtained (at 77 K) on Accelerated Surface Area and Porosimetry analyzer ASAP 2020 (Micromeritics). The sample was activated at 200 °C for 24 h in dynamic vacuum before the measurement. Pore volumes were calculated at P/P_0 = 0.5 and taking into account the density of liquid N_2 at 77K.[52-53]

Adsorption isotherms were simulated with the "adsorption isotherm" task within the "Sorption Tools" menu in BIOVIA Materials Studio version 2017r2. The simulations were performed at 77 K, using a geometry optimized N_2 molecule as the adsorptive and a single, geometry-optimized unit cell of the model structure of interest as the adsorbent. We adopted the Metropolis method and the COMPASS force field. The isotherms were simulated over a pressure range of 0.01−100 kPa, in which 50 fugacity steps were distributed logarithmically in order to increase the number of data points in the steep initial portion of the isotherm. The "Fine" quality setting was used for all simulations. Charges were force field assigned, while electrostatic forces were calculated with the Ewald method. The "atom-based" method was adopted for the calculation of van der Waals forces. No constraints were assigned.

Zirconium K-edge XANES and EXAFS spectra were measured using Rigaku R-XAS spectrometer installed in the "Smart Materials" center of the Southern Federal University, Russia. Bremsstrahlung was produced by an X-ray tube with fixed water-cooled W anode operating at 30 kV and 70 mA. White beam was monochromatized by Johansson-type Si(620) crystal with energy resolution of around 15 eV at 18 keV. The samples in powder form were pressed into pellets of 18 mm in diameter. The mass of the samples was optimized to obtain the best signal-to-noise ratio in EXAFS spectra. Measurements were performed at room temperature in transmission mode using a single scintillation counter as a detector. Total acquisition time per sample was around 3.5 h. Subsequent data treatment was carried out in Athena code of Demeter package.[57]

The Raman spectra were collected on inVia Raman Microscope (Renishaw) on the samples in air with 785 nm laser of 0.05% power, and 20x objective. Reported spectra are the average of 30 acquisitions performed on three different points (10 each) on the sample.

Prior to NMR measurement samples were calcined in air at 200 °C for 24 h to remove solvent and physisorbed modulator. Samples were prepared by weighing 20 mg of MOF into a centrifuge tube. A 1 ml solution of 1M NaOH in D_2O was then added to the tube. Upon addition of the digestion medium, the centrifuge tubes were capped and shacked on IKA KS260 instrument for 30 min before leaving the samples to digest over a period of 24 h. This OH^- based procedure dissolves only the organic portion of the MOF (linker, modulator, solvent etc.), while the inorganic component precipitate as Zirconium dioxide. The precipitate was separated by centrifugation at 3000 rpm for 30 min and the 600 µl of top solution was sampled in NMR. Liquid ^1H NMR spectra were recorded with a Bruker Avance DPX-400 NMR Spectrometer (300 MHz). The relaxation delay (d1) was set to 20 seconds to ensure that reliable integrals were obtained, allowing for the relative concentrations of the molecular components to be accurately determined. The number of scans was 64.

3. Results and discussion

3.1. XRPD synchrotron radiation data refinement: comparison between 0BC and standard UiO-66.

Rietveld refinement of XRPD data collected at the BM01B beamline of the ESRF synchrotron on UiO-66-NDC (0BC) sample confirms that it is isoreticular to UiO-66. Being compared, the patterns show very little difference in shape and intensity of the reflections, although showing a little shift towards lower 2θ due to a small increase of the lattice parameter (from a = 20.7582(4) to 20.851(1) Å, corresponding to $\Delta a \approx +0.093$ Å, $\Delta a/a = +0.45$ %, see Figure 1 and Table 2 and Table 3). The increased value of lattice constant in UiO-66-NDC is related to the stress created by extra benzene rings of the 1,4-NDC molecules in comparison with the standard BDC ligands.

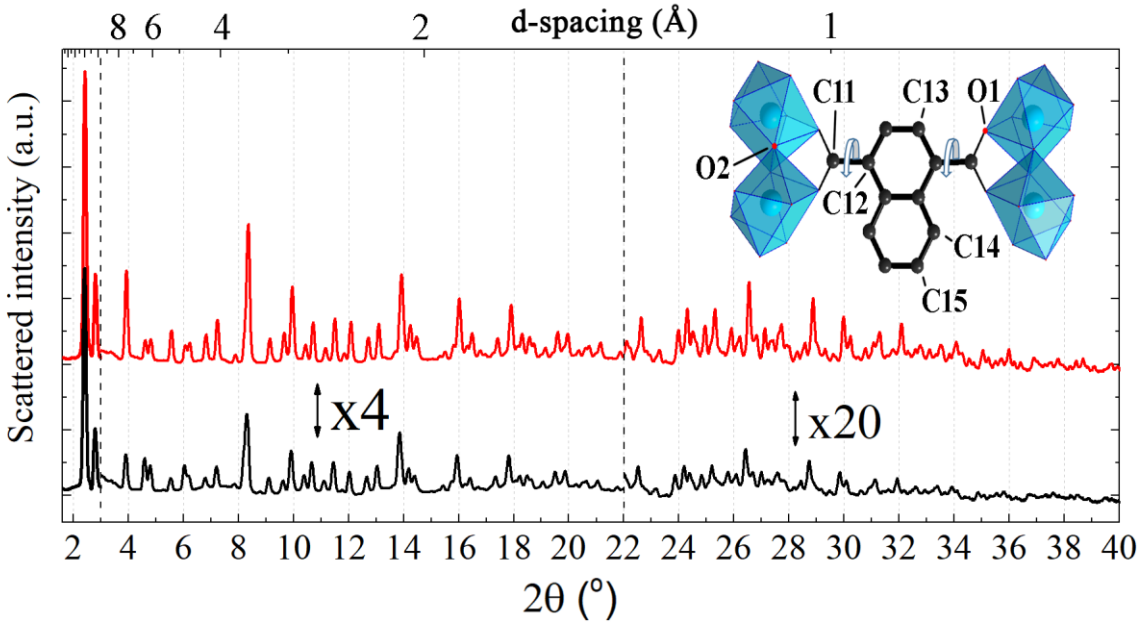

Figure 1. Background corrected XRPD patterns of UiO-66 (red) and UiO-66-NDC-0BC (black) samples obtained using synchrotron irradiation: λ = 0.505235(5) Å. To better appreciate the higher 2θ angle data, the patterns have been multiplied by a factor 4 and 20 in the 3–22 ° and 22–40 ° 2θ-intervals, respectively. The model in the top right corner depicts connection of linker with SBU in UiO-66-NDC structure. Blue polyhedra represent zirconium coordinated by oxygen ions, while the carbon atoms of the linker are represented by black spheres; σ-bonds are denoted by white flat arrows. Also reported are the labels used in the refinement to discriminate among crystallographic independent carbon and oxygen atoms, see Table 2 and Table 3.

The Rietveld refinement of the UiO-66 MOF was performed in the *Fm-3m* space group (N. 225) using as starting model the structure refined in the original manuscript of Cavka *et al.*[19] (that combined XRPD and Zr K-edge EXAFS data) and fixing to unit the occupancy factors of all atoms, see Table 2. Because of the high symmetry of the space group, the structure contains only one

independent zirconium atom, two independent oxygen atoms (O2 being the μ3-O atom of the inorganic cornerstone and O1 belonging to the carboxylate unit of the linker) and three carbon atoms of the BDC linker (C11, C12 and C13; C14 and C15 are present only in NDC linker), see inset in Figure 1 and Table 2.[19, 21, 25] A quite large isotropic atomic displacement parameter was found for C13 (Uiso = 0.077(5) Å^2) with respect to that of C11 and C12 atoms. This could be interpreted as a small twisting of the benzene ring of the BDC linker around the σ-bonds between C11 and C12. Such twisting would not affect the time averaging of the electron density of C11 and C12, being on the rotation axis, while that of C13 would result in a clearly anisotropic atomic displacement, difficult to clearly put in evidence from XRPD data. Another possible explanation would be that the benzene ring of the BDC linker would have an out of plane equilibrium position. If this would be the case the C13 atom should have a y coordinate different from zero, half of the occupancy and double degeneration for symmetry reasons. This is indeed the situation found by the recent single crystal synchrotron radiation X-ray diffraction reported by Øien *et al*.[25] Being the C13 atom quite close to the rotation axis, such twisting effect (if present) is relatively small and we are unable to confirm or discard the result of Øien *et al*.[25] from our XRPD data. As the refinement obtained with the simpler model reported in the original work of Cavka *et al*.[19] was able to properly reproduce the experimental XRPD pattern, we decided to keep this higher symmetry model. The comparison between observed, calculated, and difference (black, red and blue line, respectively) XRPD patterns has been reported in Figure 2a.

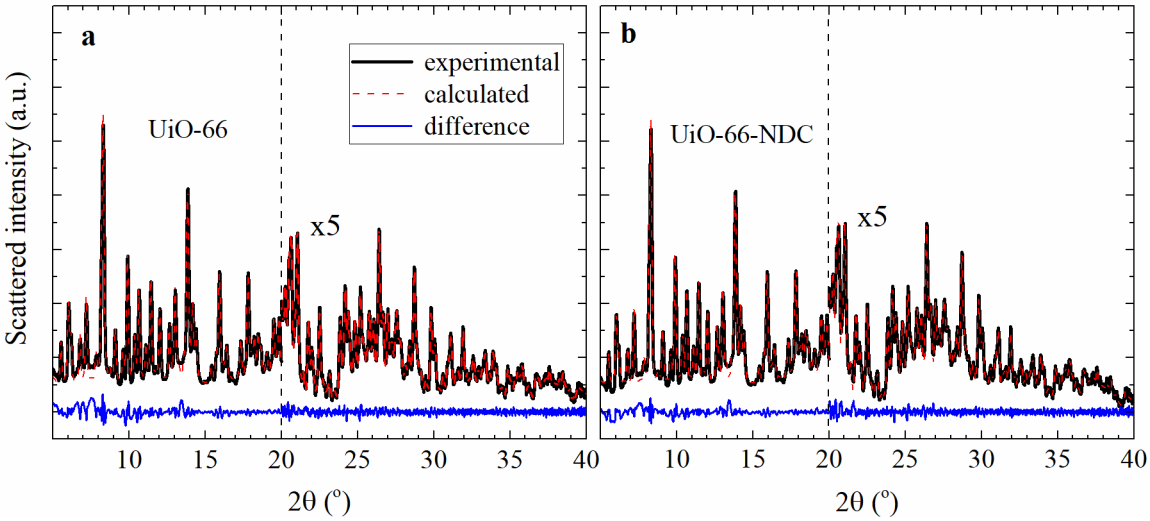

Figure 2. Part (a): Observed (black line), calculated (red line), and difference (blue line) XRPD patterns for the UiO-66 MOF: λ = 0.505235(5) Å. Part (b): as part (a) for the UiO-66-NDC-0BC MOF. The quantitative results of the two Rietveld refinements are reported in Table 2 and Table 3, respectively.

Table 2. Atomic parameters resulting from the Rietveld Refinement of the UiO-66 in the *Fm-3m* space group (N. 225): fractional coordinates (x, y, z); isotropic atomic displacement parameters (Uiso), occupancy factors, site degeneration and number of atoms in the unit cell. To compare with the previous refinement,[19] please consider that Uiso = Beq/(8π^2). Values of Rwp and Rp parameters are 0.86 and 0.82, respectively, and reduced χ^2 = 2.13 for 40 variables. The refined cell parameter is *a* = 20.7582(4) Å [V = 8944.8(6) Å^3]. See the inset in Figure 1 for the atom labeling.

atom	x	y	z	Uiso (Å^2)	Occupancy factor	site	N of atoms /unit cell
Zr	0.1198(1)	0	0	0.0116(4)	1.000	24e	24
O1	0.1750(3)	0	0.0919(3)	0.022(2)	1.000	96j	96
O2	0.0555(3)	–x	–x	0.018(3)	1.000	32f	32
C11	0.1467(4)	0	–x	0.035(5)	1.000	48h	48
C12	0.2044(5)	0	x	0.065(7)	1.000	48h	48
C13	0.2686(6)	0	0.1772(6)	0.077(5)	1.000	96j	96

The same strategy adopted to refine the data of UiO-66-NDC-0BC succeeded in locating Zr, O1, O2, C11, C12, C13 in reasonable positions with physically meaningful Uiso parameters, but failed in

locating C14 and C15 with y fixed to 0. Indeed, when we tried to refine the corresponding occupancy factors, they resulted to almost null values. We then adopted the model reported by Øien *et al.*,[25] removing the constrains on the y ordinate of C13, C14 and C15 atoms. To guarantee stability to the refinement we applied soft constrains to the C12, C13, C14 and C15 atoms to stay on the same plane. Soft constrains have also been adopted on all C=C distances between aromatic carbons (around 1.4 Å) and between C11 and C12 (around 1.5 Å, single-bond distance). The refinement stability further improved by adding a soft constrain on the O1-C11-O1 angle around 126 °, that defines the connection between the linker and the inorganic cornerstone.
The occupancy factors of the atoms of the inorganic cornerstone have been fixed to unit, while those of the atoms of the NDC linkers were fixed to 0.87 according to the TGA data (see below Figure 9). The result of the refinement is reported in Table 3, the structure of the NDC linker is reported in Figure 3, while the comparison between observed, calculated, and difference (black, red and blue line, respectively) XRPD patterns can be appreciated in Figure 2b.
Repeating the last refinement fixing to unit we obtained results fully compatible with those presented here, as the atomic coordinates for all atoms are equivalent in both refinements within less than 2 estimated standard deviations (esd). The simulated pattern still resulted in a good agreement with the experimental one, but the all the Uiso of the carbon atoms slightly increased and the fit goodness factors worsen by about 5% with respect to the results reported in Table 3. We consequently decided to consider as final refinement that obtained by fixing the occupancies of the atoms of the NDC linkers to 0.87. See section S1 and table S1 of the SI for a more detailed comparison between the two refinements.

Table 3. Atomic parameters resulting from the Rietveld Refinement of the UiO-66-NDC-0BC MOF in the *Fm-3m* space group (N. 225): fractional coordinates (x, y, z); isotropic atomic displacement parameters (Uiso), occupancy factors, site degeneration and number of atoms in the unit cell. Values of Rwp and Rp parameters are 0.76 and 0.81, respectively, and reduced $\chi^2 = 1.55$ for 45 variables. The refined cell parameter is $a = 20.851(1)$ Å [$V = 9065(1)$ Å^3]. See the inset in Figure 1 for the atom labeling. The occupancy factors of the atoms of the inorganic cornerstone have been fixed to unit, while those of the atoms of the NDC linkers were fixed to 10/12 according to the TGA data (see below Figure 9). The refined structure has been deposited in the CCDC data base with number 1553924.

atom	x	y	z	Uiso (Å^2)	Occupancy factor	site	Atoms/unit cell
Zr	0.1176(1)	0	0	0.0129(8)	1.00	24e	24
O1	0.1699(3)	0	0.0903(3)	0.022(2)	1.00	96j	96
O2	0.0641(4)	−x	−x	0.056(5)	1.00	32f	32
C11	0.1504(2)	0	−x	0.003(4)	0.87	48h	41.76
C12	0.2012(2)	0	x	0.043(7)	0.87	48h	41.76
C13	0.2603(3)	0.0280(5)	0.1890(3)	0.023(6)	0.435	192l	83.52
C14	0.2724(5)	0.056(1)	0.1296(4)	0.24(3)[a]	0.217	192l	41.76
C15	0.3317(7)	0.084(2)	0.1174(6)	0.36(5)[a]	0.217	192l	41.76

[a] An unique Uiso parameter for C14 and C15 atoms was set proportional to the distance from the rotational axis.

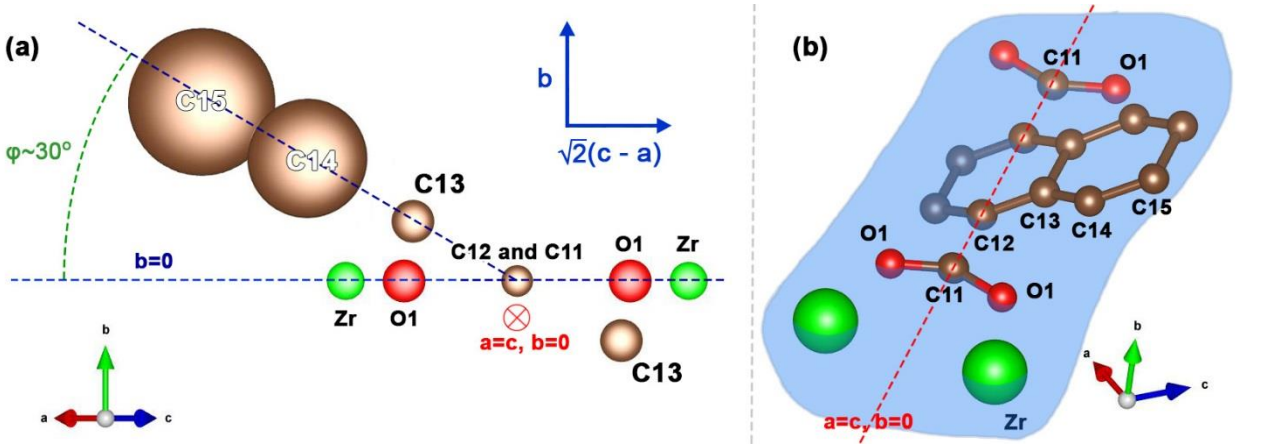

Figure 3. Part (a) View from the (101) direction of the atoms of the NDC linker as optimized in the refinement reported in Table 3. For each atom, the radius of the spheres is defined by the corresponding $(Uiso)^{1/2}$ value. For symmetry reasons four equivalent values of the φ angle are available: φ = +30, –30, +150 and –150 (only the first solution is here represented). Part (b): analogous representation of the same optimized structure reported from a tilted view. In this case the sphere radii correspond to the atomic radii and do not consider the thermal motion. In both parts, the 3-dimensional visualization of crystal structure was performed using the VESTA code.[58]

For symmetry reasons four equivalent values of the φ angle are available: φ = +30, –30, +150 and –150; for graphical reasons, only the φ = +30 case has been represented in Figure 3a. From this picture, it becomes evident why the first refinement, performed fixing y = 0 for the C13, C14 and C15, resulted in locating only C13, with a larger Uiso parameter with respect to that of C11 and C12 atoms. Indeed, if we label as C13', C14', and C15' the carbon atoms of the NDC linker corresponding to the φ = –30 solution, then the relative distances of the symmetry equivalent atoms are: 1.21, 2.42 and 3.63 Å for d(C11–C11'), d(C12–C12') and d(C13–C13'), respectively. This implies that only the couple of C13 and C13' have some electron density on the y = 0 plane, while C14, C14' and C15 and C15' are too far from that plane. The optimized Uiso parameters (Table 3) exhibit the following trend: C11 < C12 < C13 < C14, C15. This observation suggests a small twisting of the NDC rings around the equilibrium position (φ = +30, –30, +150 or –150).

Summarizing, our synchrotron radiation XRPD study confirmed that UiO-66-NDC (0BC) sample is isoreticular to UiO-66 and evidenced that the NDC ligand adopts a tilted position of φ = 30°, a value that is indeed comparable to the torsion angles found in molecular structures of napthtyl carboxylates and carboxylic acids, which is usually 10 to 40 ° interval.[59-63]

For the standard UiO-66 analogue, the BDC ligands are free to occupy the high symmetry position (φ = 0 °), see Figure 4a. Conversely, using the more bulky NDC ligands, in the UiO-66-NDC framework there is a steric conflict between the naphthyl groups of two adjacent linkers (Figure 4b), that forces carboxylate and naphthyl groups of the same linker to be out of plane. The torsional angle optimized in the present XRPD refinement (φ = 30 °, see Table 3) is stabilized by the optimization of an attractive interaction between a σ orbital of a C–H group and the π orbital of two naphthyl groups in two adjacent linkers (Figure 4c). It is worth noticing that this tilting effect is even more pronounced in the case of the UiO-67 analogue (φ = 36 °),[28] where the φ value confirms the tendency of binaphthyl to have high torsion angles, due to intramolecular interactions, see Figure 4d. It is finally worth considering that neutron powder diffraction would have been a much more suitable technique to obtain a more accurate location the linker atoms than XRPD (which scattering is dominated by the Zr atoms),[64] however, the much larger sample amount requested (from some mg to few g), and the need to use deuterated linkers in the synthesis prevented the use of such strategy. Notwithstanding this evidence, the accuracy of our synchrotron radiation XRPD study is sufficient to evidence the tilted position of the ligand.

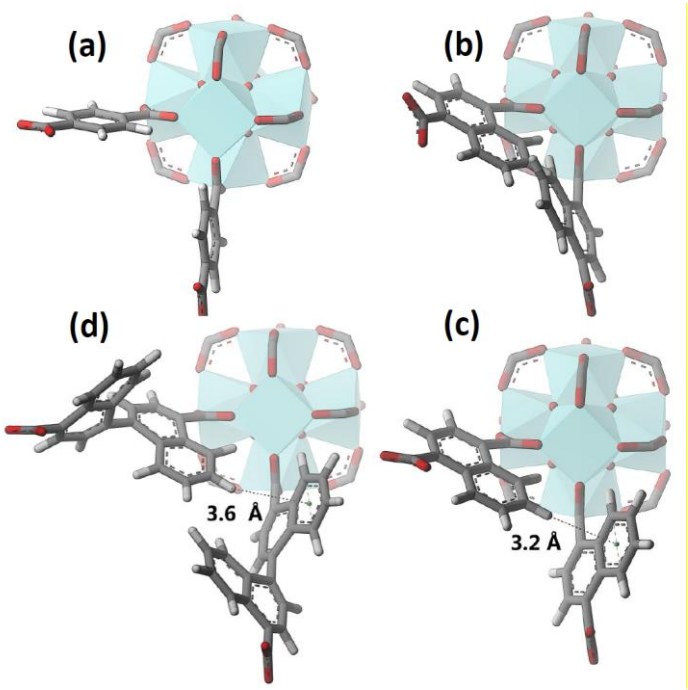

Figure 4. Graphical representation of the inorganic $Zr_6(OH)_4O_4$ SBU with two adjacent linkers in some different UiO-66- and UiO-67-type structures. Part (a) Standard UiO-66 (BDC ligand), from single crystal XRD refinement ($\varphi \sim 0$ °).[25] Part (b): picture showing the overlap between adjacent NDC ligands in case of a too small value of the torsional angle φ for UiO-66-NDC. Part (c): UiO-66-NDC, optimized from XRPD ($\varphi = 30$ °), this work. Part (d): UiO-67-BN (3,3′-dimethylbiphenyl and 1,1′-binaphthyl linker scaffolds), from single crystal XRD refinement ($\varphi = 36$ °).[28]

3.2. Crystal size and textural properties

The materials crystallize in intergrown crystals (shown in Figure 5) which are too small (<1 μm) for structure determination by single crystal diffraction. From the SEM images it emerges that higher amount of BC leads to the formation of larger crystals with better defined morphology. The average size increases from 80, through 150 up to 800 nm for 0BC, 10BC and 60BC, respectively. Without addition of BC intergrown aggregates of very small crystals are observed, and the shape of 0BC crystals is not well established (Figure 5a). On the contrary, addition of 10 or 60 equivalents of BC results in well-defined octahedral crystals (Figure 5b,c). It is also evident from the images that one crystal is formed on the facet of another.

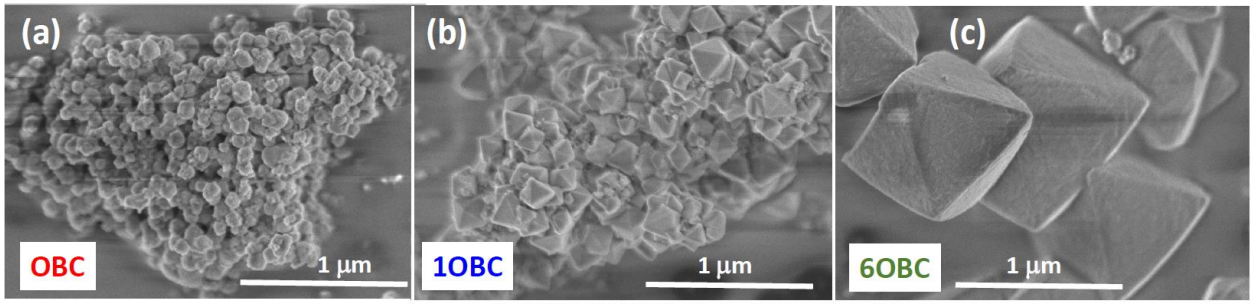

Figure 5. SEM micrographs of 0BC, 10BC and 60BC samples, parts (a), (b) and (c), respectively. All images were taken with the same magnification.

XRPD patterns of UiO-66-NDC structure with variation of modulator content are shown in Figure 6. The intensities of XRPD reflections become sharper with increase of BC amount, evidencing different crystallinity of the samples. Reflections due to planes with similar *d*-spacing could be best resolved in 60BC sample. For example, the (315) and (006) reflections in the 8.2-8.5° 2θ region can be distinguished starting from 0BC sample, but they are becoming fully split only in 60BC pattern.

Moreover, the (339) and (608) reflections, in 14.0-14.2° 2θ region, and (719) and (828) reflections, in 16.1-16.3° 2θ region, are merged to single peak for the 0BC sample, and resolved in the 60BC pattern, which is demonstrated in the insert of Figure 6. The FWHM of (317) reflection at ~10.8° decreases from 0.063° for sample synthesized without BC modulator to 0.046° for 60BC sample. The limiting resolution of the setup obtained for a standard LaB_6 (NIST) sample is 0.042° FWHM for (101) reflection at 10°. Cell parameters are decreasing from 20.851 Å for 0BC sample to 20.827 and 20.820 Å for 10BC and 60BC, respectively, as determined by Rietveld refinement of the XRD patterns. This means that the progressive addition of modulator decreases the stress created by the use of 1,4-NDC linkers instead of the standard BDC for the UiO-66 synthesis, resulting in a = 20.7582(4) Å, see Table 2.

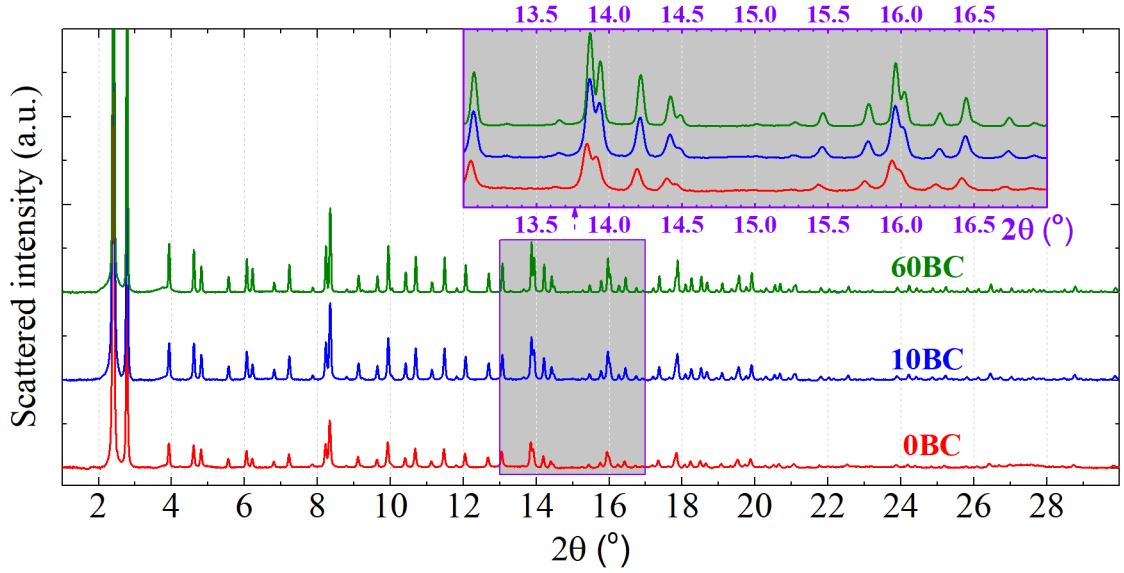

Figure 6. XRPD patterns of UiO-66-NDC samples prepared with different amount of BC modulator, from bottom to top: 0BC (red), 10BC (blue) and 60BC (olive): λ = 0.505235(5) Å. The insert reports a magnification of the 13–17° 2θ region.

3.3. N_2 adsorption isotherms

For the UiO-66, 67 and 68 family of MOFs, the increase of crystal size with addition of modulator was previously described[43] and can be explained by the fact, that zirconium ions form a complex salt with BC. The presence of BC in the synthesis batch changes the reaction mechanism, because all active sites around Zr^{4+} ions became occupied with BC molecules. In such situation, any linker molecule can interact with zirconium ion only via exchange reaction. This fact decreases the rate of nucleation in solution and, therefore, results in bigger crystals. It should be mentioned that another process could also take place. If concentration of a monobasic acid in solution is much higher than that of a linker, an exchange reaction might be suppressed. As the result, a portion of SBUs will keep molecules of modulator coordinated to metal ion instead of being available for coordination of linker. Since monobasic acids can contact zirconium in one SBU only (while linker molecules can connect two adjacent SBUs, compare parts (a) and (b) of Figure 7.

Depending on the number of vacancies this feature may increase the surface area, the pore volume and reduce stability of the material, as demonstrated by Shearer *et al.*[24] where the linker vacancies were tuned by acting on the synthesis temperature and on the $ZrCl_4$/BDC ratio. Linker vacancies may yield to Zr ions characterized by two coordination vacancies thus representing surface Lewis acid centers of potential catalytic interest.[8-10] When the BC/NDC ratio is high it may be possible that some $Zr_6O_4(OH)_4$ cornerstones are missing: this happens when most of the adjacent ones are capped by BC units, as schematically shown in Figure 7c. Finally, by further increasing the BC/NDC ratio (see the 100BC case in Table 1), most of the 12 connections of the SBU are capped by BC preventing the crystallization process.

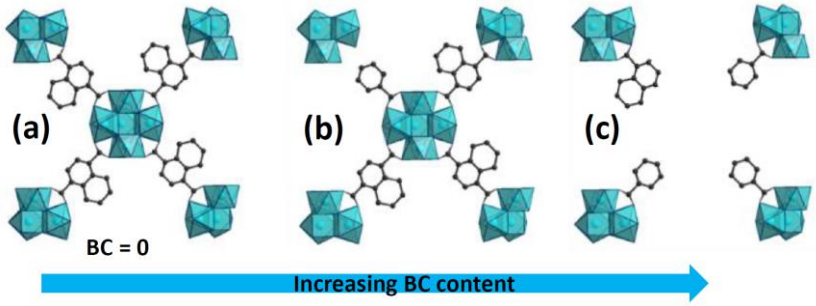

Figure 7. Qualitative scheme of defect formation in synthesis with increasing amount of BC acid. (a) Perfect case (absence of BC acid). (b) Formation of little pores (small amount of BC acid). (c) Formation of big pores, with missing clusters (large amount of BC acid).

The presence of an increasing density of cornerstone vacancies upon increasing the BC content in the synthesis (hypothesized in Figure 7) is confirmed by the N_2 adsorption isotherms reported in Figure 8a (scattered curves), that clearly show that the adsorption plateau appears at significantly higher cm^3 g^{-1} STP values moving from 0BC to 10BC and 60 BC. The consequent Barrett-Joyner-Halenda[65] (BJH) pore size distribution is shown in Figure 8b,c as determined from adsorption and desorption isotherms, respectively.[66] All samples are exhibiting similar sorption profile and the isotherms can be attributed to the type I (IUPAC classification), which is typical for micropous materials. Specific surface area calculated by Brunauer-Emmett-Teller (BET)[67] and Langmuir[68] models increases with amount of BC and the same occurs for the pore volumes (Table 1), supporting the defective models schematized in Figure 7b,c: see the distribution of nanopores in the 2-3 nm region (Figure 8b,c). For microporous materials the region of the isotherm near to $P/P_0 = 1$ is usually ascribed to adsorption in cavities between the crystallites of material. Respectively to what is observed in Figure 8a, the isotherm of 10BC sample demonstrates the highest adsorption, while that of 60BC has no evident increment. This situation is well illustrated by the SEM image shown in Figure 5c, showing well separated big crystals, leaving almost no cavities between them. In case of 0BC sample (Figure 5a) the smaller crystallites exhibit a more dense packing in comparison to 10BC sample (Figure 5b), which leaves no significant free volume between the crystallites.

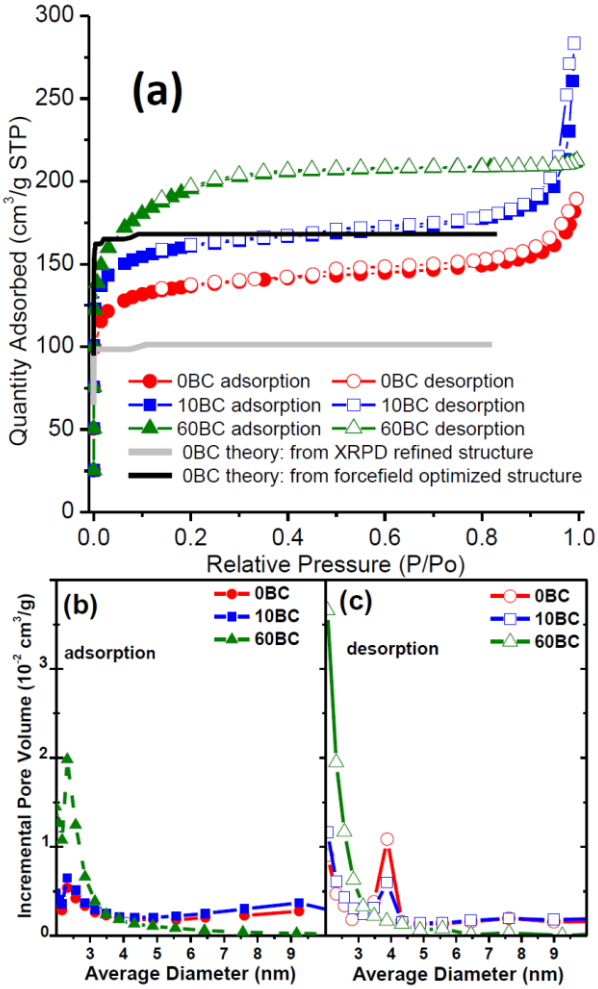

Figure 8. Part (a): N_2 physisorption isotherms of 0BC (circles), 10BC (squares) and 60BC (triangles) samples. The filled and open symbols represent the adsorption and desorption branches, respectively. Also reported are the theoretical adsorption curves calculated on the structures obtained from XRPD refinement (gray line) and from a subsequent forcefield optimization (black curve). Part (b): BJH adsorption pore distribution obtained from the N_2 physisorption isotherms reported in part (a). Part (c) as part (b) from the desorption isotherms.

The presence of the cornerstone vacancies (hypothesized in Figure 7) in the 60NDC sample is further confirmed by the edge jump of the Zr K-edge study reported in Section S3 of the SI (see Figure S2a) and quantified it to about 15%. The EXAFS data analysis (Figure S2b-d) confirms the similarity of the SBU in the 0BC and 60BC materials compared to a standard UiO-66 material. This testifies that the local environment of Zr is the same in all samples and corresponds to that of the standard UiO-66 sample.[19, 21] Coming back to the diffraction data (Figure 6), the absence of the forbidden reflections[24, 29, 31, 37] in the small angle region implies the absence of long range order in the structural defects.

Of interest are the full line curves in Figure 8a, reporting the simulated adsorption isotherms for the framework optimized by XRPD refinement (gray curve) and after a successive forcefield optimization of the structure (black curve, see above Section 2.2 for details). The UiO-66-NDC framework, considered as a rigid entity is not able to justify the N_2 uptake measured in the experiment (gray full curve). This uptake increases significantly when the structure is allowed to relax (black full curve). This simulation puts in evidence the flexibility of the rotation of the NDC ligands around the torsional φ angle and justifies the high Uiso parameters obtained in the Rietveld refinement for C14 and C15 atoms, see Table 3.

3.4. Thermal stability by TGA and XRPD

It is now well established that the UiO-66 framework is incredibly tolerant to a high concentration of defects. The initial evidence for this came in the form of TGA data presented in a paper by Valenzano *et al*.[21] Therein, the authors demonstrated that the magnitude of the decomposition weight loss step was significantly less than that theoretically expected by the idealized chemical equation $[Zr_6O_6(BDC)_6] \rightarrow 6\ ZrO_2$. The TGA of all samples are reported in Figure 9 by rescaling the weight at the end of the process to 100% and attributing it to the pure ZrO_2 phase (non-scaled TGA curves are reported in Figure S3). The theoretical weight loss from the burning of the organic linkers are in the case of defect-free 1,4-NDC 161% based on ZrO_2, this weight is indicated as a dotted line in Figure 9. The sample made without modulator, 0BC, has a weight loss upon combustion that corresponds to 13% missing linkers. On these basis, we fixed to 0.87 the occupancy factor of the atoms of the NDC linker in the Rietveld refinement of 0BC, see Section 3.1, Table 3. The samples made with benzoic acid as modulator demonstrate a larger and less sharp weight loss. This is probably due to "missing cluster defects" (Figure 7c), as it is known from a parallel study on UiO-66, that are promoted by modulated synthesis.[31, 41] This evidence, confirmed by the Zr K-edge jump in XAS experiment (see SI Figure S2), underlines that the formation of missing SBUs (Figure 7b,c) is more effective at higher BC content. The framework breakdown temperature follows the trend (60BC < 10BC < 0BC) as evidenced by the extend of the stability plateau (250-450 °C interval) and as clearly observed in the temperature dependent XRPD pattern collected after heat treatment in air at 200, 300, 400, and 500 °C for 12 h (Figure 10). Samples 0BC and 10BC preserve their initial structure up to 400 °C. However, at this temperature partial decomposition of the structure of 10BC sample can be observed (see widening of the reflexes in Figure 10b). Sample 60BC maintained crystallinity up to 200 °C only (Figure 10c), while at 300 and 400°C broad XRD peaks indicate the loss of long range order. All samples collapsed at 500 °C into ZrO_2. However, even most temperature unstable 60BC sample could be activated for potential applications (solvent removal) without losing its initial structure.

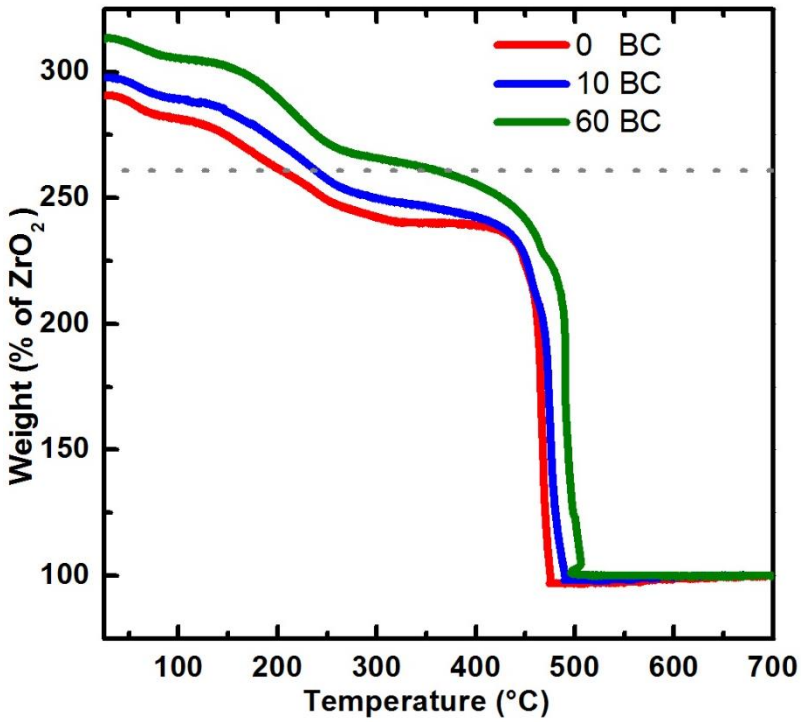

Figure 9. TGA plots showing the thermal degradation of 0BC, 10BC and 60BC samples renormalized referring the remaining weight at high temperature (ZrO_2) as 100 %. Under this convention, the weight of a desolvated UiO-66 free of defects should be 161 % (see doted grey line).

Due to possible technologic application (i.e. sorption and catalysis) of the material, water stability tests were performed. All samples preserved their crystal structure after contact with water at room temperature for 24 h and subsequent activation at 200 °C for 12 h (see SI, Figure S1).

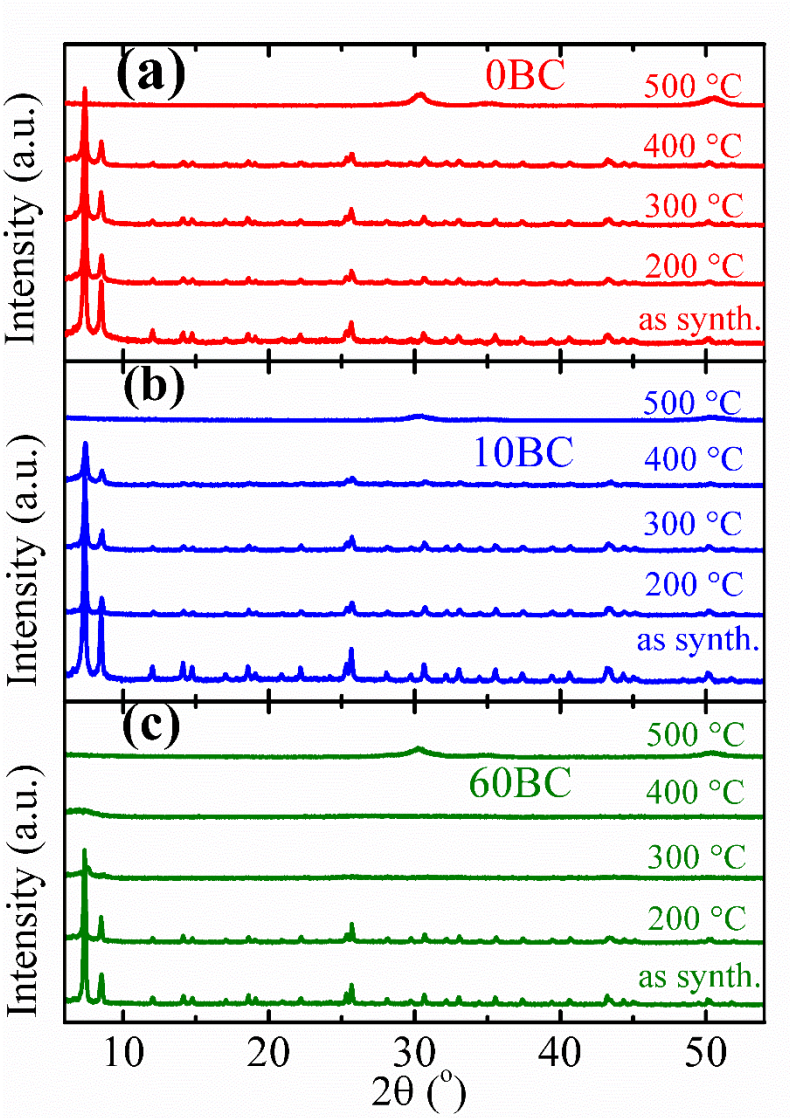

Figure 10. XRPD patterns of 0BC, 10BC, 60BC samples recorded at room temperature after thermal treatment in air, parts (a) to (c), respectively. From bottom to top: as synthesized and heat treatment 200 °C, 300 °C, 400 °C, 500 °C for 12 h. In the adopted ordinate scale, the intensity of the low 2θ reflections are cut for graphical reasons. Patters have been collected with Cu Kα radiation (λ = 1.5406 Å).

3.5. Incorporation of BC modulator in the framework determined by dissolution-^{1}H NMR and Raman

As deeply described in the works of Shearer *et al.*[29, 31, 37] the dissolution-^{1}H NMR technique allows to identify and quantify the organic components of a MOF (e.g. linker, modulator, or pore-filling solvent) dissolving the MOF in a deuterated digestion medium and successive liquid ^{1}H NMR spectroscopy. Figure 11a reports the liquid ^{1}H NMR spectra of 10BC and 60BC, compared with those measured on 1,4-NDC linker and BC modulator. The quantitative integration of the area of the specific NMR peaks in the 7.75-7.65 and 8.10-8.00 ppm regions for the BC and 1,4-NDC, respectively, resulted in a BC/1,4-NDC ratio of 0.28 and 0.47 for 10BC and 60BC samples, respectively.

This result is qualitatively confirmed by Raman spectroscopy (Figure 11b), where the most intense Raman band of the BC modulator (corresponding to a ring deformation mode at 1005 cm^{-1}) is absent

in 0BC sample and progressively increases from 10BC to 60BC. A complete spectroscopic (IR and Raman) characterization of the vibrational properties of linkers and modulators used in the synthesis of modified versions of UiO-66, supported by periodic DFT calculations, has recently been reported by Atzori *et al.*,[31] and we refer to that work for a complete assignment of the bands present in Figure 11b. Moreover, it is clear that benzoic acid was completely removed by the adopted washing procedure, since key bands (such as the ν(C=O) and ν(C-O) evidenced by • symbol) are completely absent from the UiO-66 spectra.

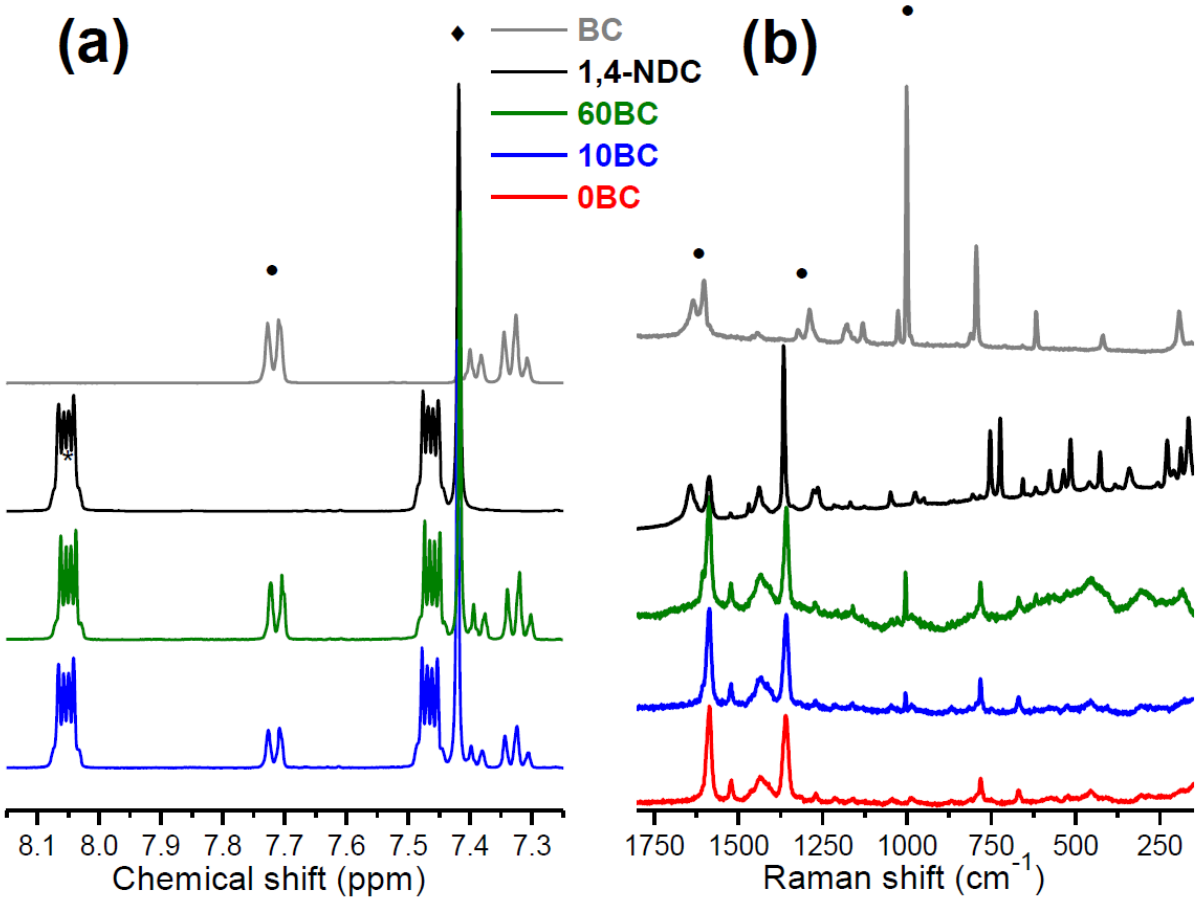

Figure 11. Part (a): Dissolution ^{1}H-NMR spectra obtained on the BC-modulated UiO-66-NDC MOFs. Also reported for comparison are the reference spectra of 1,4-NDC linker and BC modulator (black and gray curve, respectively). All spectra except BC are normalized to the peak 7.4 ppm shown by ♦. The • and * show the peaks used to calculate the BC to 1,4-NDC ration. MOF samples were activated 200 °C for 24h in air prior NMR measurement. Part (b) Raman spectra of 0BC, 10BC, 60BC samples, collected with λ = 785 nm. For comparison, also reported is the spectrum of BC and 1,4-NDC (collected with λ = 514 nm and 785 nm, respectively). In the BC spectrum, marker bands of ν(C=O) and ν(C-O) of the carboxylic acid are underlined by the • symbol, together with the most intense Raman band due to the ring deformation at 1005 cm^{-1}. In both parts spectra were vertically shifted for clarity.

4. Conclusions

Summarizing, UiO-66-NDC was synthesized using solvothermal method in DMF. XRPD refinement of synchrotron radiation data highlighted that the naphthalene rings of the NDC linker is out of (a,c)-plane equilibrium by 30 °, adopting a geometry that maximizes the attractive interaction between a σ orbital of a C–H group and the π orbital of two naphthyl groups in two adjacent linkers. The influence of BC modulator agent was investigated changing the BC/NDC linker fraction from 0 to 60. No nucleation was observed for BC/NDC = 100. Larger amounts of BC results in formation of bigger octahedral crystals of UiO-66-NDC (due to decrease of crystal growth kinetics) characterized by an increased specific surface area (due to formation of more defects in the lattice). For all crystalline

samples XRPD and EXAFS confirmed the target structure on both long- and short-range order grounds. TGA and XRPD analyses revealed decrease of thermal stability with increase of modulator amount: the presence of both linker and SBU defects is the origin of the loss of stability, the latter being more important at higher BC content. Remarkably, all samples prepared with and without modulator are stable in water even after reactivation. Thus UiO-66-NDC, and its defective derivatives synthesized upon increasing the BC/NDC ratio, are sufficiently stable to be fully desolvated and represents good candidates for further functionalization with active catalytic centres for reactions running in gas or in liquid phases up to 200 °C.

■ ASSOCIATED CONTENT

Supporting Information

Further details on the XRPD diffractograms testifying the water stability of the materials, the Zr K-edge XANES and EXAFS study and the as collected TGA curves. This material is available free of charge via the Internet at http://pubs.acs.org.

■ AUTHOR INFORMATION

Corresponding Author

*E-mails: vbutova@sfedu.ru; carlo.lamberti@unito.it

Notes

The authors declare no competing financial interest.

■ ACKNOWLEDGMENTS

VVB, APB, AAG, KAL, ALB, AVS, and CL acknowledge Mega-Grant of Ministry of Education and Science of the Russian Federation (14.Y26.31.0001) for funding the research. AAG acknowledges the grant of the President of Russia for young scientists MK-7300.2016.2. We are indebted to Vladimir Dmitriev, Herman Emerich, Wouter van Beek, and Michela Brunelli for the friendly and competent support during the experiment performed at the BM01B (now BM31) beamline of the ESRF. We acknowledge the support of Alessandro Damin during the Raman experiments. The authors are grateful to Boris Bouchevreau for helpful discussion.

Supporting information

The Supporting Information is available free of charge on the ACS Publications website at DOI:
Additional Rietveld refinement of the XRPD pattern of sample 0BC performed fixing all site occupancy factors to unit; XRPD patterns on water stability tests of the different MOFs; Zr K-edge X-ray absorption study; raw TGA data.

REFERENCES

1. Furukawa, H.; Cordova, K. E.; O'Keeffe, M.; Yaghi, O. M. *Science* **2013,** *341*, Art. n. 1230444.
2. Kaskel, S.; Ed. *The Chemistry of Metal-Organic Frameworks: Synthesis, Characterization, and Applications*. John Wiley & Sons: Weinheim, 2016.
3. Li, J. R.; Kuppler, R. J.; Zhou, H. C. *Chem. Soc. Rev.* **2009,** *38*, 1477-1504.
4. Murray, L. J.; Dinca, M.; Long, J. R. *Chem. Soc. Rev.* **2009,** *38*, 1294-1314.
5. Farrusseng, D.; Ed. *Metal-Organic Frameworks: Applications from Catalysis to Gas Storage*. Wiley: Weinheim, 2011.
6. Sumida, K.; Rogow, D. L.; Mason, J. A.; McDonald, T. M.; Bloch, E. D.; Herm, Z. R.; Bae, T. H.; Long, J. R. *Chem. Rev.* **2012,** *112*, 724-781.
7. Ma, L. Q.; Abney, C.; Lin, W. B. *Chem. Soc. Rev.* **2009,** *38*, 1248-1256.
8. Corma, A.; Garcia, H.; Xamena, F. *Chem. Rev.* **2010,** *110*, 4606-4655.
9. Ranocchiari, M.; van Bokhoven, J. A. *Phys. Chem. Chem. Phys.* **2011,** *13*, 6388-6396.

10. Llabres i Xamena, F. X.; Gascon, J. *Metal Organic Frameworks as Heterogeneous Catalysts*. Royal Society of Chemistry: Cambridge, 2013.
11. Chughtai, A. H.; Ahmad, N.; Younus, H. A.; Laypkov, A.; Verpoort, F. *Chem. Soc. Rev.* **2015,** *44*, 6804-6849.
12. Horcajada, P.; Gref, R.; Baati, T.; Allan, P. K.; Maurin, G.; Couvreur, P.; Ferey, G.; Morris, R. E.; Serre, C. *Chem. Rev.* **2012,** *112*, 1232-1268.
13. He, C. B.; Liu, D. M.; Lin, W. B. *Chem. Rev.* **2015,** *115*, 11079-11108.
14. Kitagawa, S.; Kitaura, R.; Noro, S. *Angew. Chem.-Int. Edit.* **2004,** *43*, 2334-2375.
15. Ferey, G. *Chem. Soc. Rev.* **2008,** *37*, 191-214.
16. Fang, Z. L.; Bueken, B.; De Vos, D. E.; Fischer, R. A. *Angew. Chem.-Int. Edit.* **2015,** *54*, 7234-7254.
17. Furukawa, H.; Muller, U.; Yaghi, O. M. *Angew. Chem.-Int. Edit.* **2015,** *54*, 3417-3430.
18. Butova, V. V.; Soldatov, M. A.; Guda, A. A.; Lomachenko, K. A.; Lamberti, C. *Russ. Chem. Rev.* **2016,** *85*, 280-307.
19. Cavka, J. H.; Jakobsen, S.; Olsbye, U.; Guillou, N.; Lamberti, C.; Bordiga, S.; Lillerud, K. P. *J. Am. Chem. Soc.* **2008,** *130*, 13850-13851.
20. Chavan, S.; Vitillo, J. G.; Uddin, M. J.; Bonino, F.; Lamberti, C.; Groppo, E.; Lillerud, K. P.; Bordiga, S. *Chem. Mat.* **2010,** *22*, 4602-4611.
21. Valenzano, L.; Civalleri, B.; Chavan, S.; Bordiga, S.; Nilsen, M. H.; Jakobsen, S.; Lillerud, K. P.; Lamberti, C. *Chem. Mat.* **2011,** *23*, 1700-1718.
22. Chavan, S.; Vitillo, J. G.; Gianolio, D.; Zavorotynska, O.; Civalleri, B.; Jakobsen, S.; Nilsen, M. H.; Valenzano, L.; Lamberti, C.; Lillerud, K. P.; Bordiga, S. *Phys. Chem. Chem. Phys.* **2012,** *14*, 1614-1626.
23. Jakobsen, S.; Gianolio, D.; Wragg, D. S.; Nilsen, M. H.; Emerich, H.; Bordiga, S.; Lamberti, C.; Olsbye, U.; Tilset, M.; Lillerud, K. P. *Phys. Rev. B* **2012,** *86*, Art. n. 125429.
24. Shearer, G. C.; Chavan, S.; Ethiraj, J.; Vitillo, J. G.; Svelle, S.; Olsbye, U.; Lamberti, C.; Bordiga, S.; Lillerud, K. P. *Chem. Mat.* **2014,** *26*, 4068-4071.
25. Øien, S.; Wragg, D.; Reinsch, H.; Svelle, S.; Bordiga, S.; Lamberti, C.; Lillerud, K. P. *Cryst. Growth Des.* **2014,** *14*, 5370-5372.
26. Reinsch, H.; Bueken, B.; Vermoortele, F.; Stassen, I.; Lieb, A.; Lillerud, K. P.; De Vos, D. *Crystengcomm* **2015,** *17*, 4070-4074.
27. Øien, S.; Agostini, G.; Svelle, S.; Borfecchia, E.; Lomachenko, K. A.; Mino, L.; Gallo, E.; Bordiga, S.; Olsbye, U.; Lillerud, K. P.; Lamberti, C. *Chem. Mat.* **2015,** *27*, 1042-1056.
28. Øien-Ødegaard, S.; Bouchevreau, B.; Hylland, K.; Wu, L.; Blom, R.; Grande, C.; Olsbye, U.; Tilset, M.; Lillerud, K. P. *Inorg. Chem.* **2016,** *55*, 1986-1991.
29. Shearer, G. C.; Vitillo, J. G.; Bordiga, S.; Svelle, S.; Olsbye, U.; Lillerud, K. P. *Chem. Mat.* **2016,** *28*, 7190-7193.
30. Braglia, L.; Borfecchia, E.; Maddalena, L.; Oien, S.; Lomachenko, K. A.; Bugaev, A. L.; Bordiga, S.; Soldatov, A. V.; Lillerud, K. P.; Lamberti, C. *Catal. Today* **2017,** *283*, 89-103.
31. Atzori, C.; Shearer, G. C.; Maschio, L.; Civalleri, B.; Bonino, F.; Lamberti, C.; Svelle, S.; Lillerud, K. P.; Bordiga, S. *J. Phys. Chem. C* **2017,** *121*, 9312–9324.
32. Trickett, C. A.; Gagnon, K. J.; Lee, S.; Gandara, F.; Burgi, H. B.; Yaghi, O. M. *Angew. Chem.-Int. Edit.* **2015,** *54*, 11162-11167.
33. Goesten, M. G.; de Lange, M. F.; Olivos-Suarez, A. I.; Bavykina, A. V.; Serra-Crespo, P.; Krywka, C.; Bickelhaupt, F. M.; Kapteijn, F.; Gascon, J. *Nat. Commun.* **2016,** *7*, Art. n. 11832.
34. Lausund, K. B.; Nilsen, O. *Nat. Commun.* **2016,** *7*, 9.
35. Yang, D.; Bernales, V.; Islamoglu, T.; Farha, O. K.; Hupp, J. T.; Cramer, C. J.; Gagliardi, L.; Gates, B. C. *J. Am. Chem. Soc.* **2016,** *138*, 15189-15196.
36. Bai, Y.; Dou, Y. B.; Xie, L. H.; Rutledge, W.; Li, J. R.; Zhou, H. C. *Chem. Soc. Rev.* **2016,** *45*, 2327-2367.
37. Shearer, G. C.; Chavan, S.; Bordiga, S.; Svelle, S.; Olsbye, U.; Lillerud, K. P. *Chem. Mater.* **2016,** *28*, 3749-3761.
38. Tsuruoka, T.; Furukawa, S.; Takashima, Y.; Yoshida, K.; Isoda, S.; Kitagawa, S. *Angew. Chem.-Int. Edit.* **2009,** *48*, 4739-4743.
39. Diring, S.; Furukawa, S.; Takashima, Y.; Tsuruoka, T.; Kitagawa, S. *Chem. Mat.* **2010,** *22*, 4531-4538.
40. Umemura, A.; Diring, S.; Furukawa, S.; Uehara, H.; Tsuruoka, T.; Kitagawa, S. *J. Am. Chem. Soc.* **2011,** *133*, 15506-15513.
41. Vermoortele, F.; Bueken, B.; Le Bars, G.; Van de Voorde, B.; Vandichel, M.; Houthoofd, K.; Vimont, A.; Daturi, M.; Waroquier, M.; Van Speybroeck, V.; Kirschhock, C.; De Vos, D. E. *J. Am. Chem. Soc.* **2013,** *135*, 11465-11468.
42. Wu, H.; Chua, Y. S.; Krungleviciute, V.; Tyagi, M.; Chen, P.; Yildirim, T.; Zhou, W. *J. Am. Chem. Soc.* **2013,** *135*, 10525-10532.
43. Schaate, A.; Roy, P.; Godt, A.; Lippke, J.; Waltz, F.; Wiebcke, M.; Behrens, P. *Chem.-Eur. J.* **2011,** *17*, 6643-6651.
44. Gutov, O. V.; Hevia, M. G.; Escudero-Adan, E. C.; Shafir, A. *Inorg. Chem.* **2015,** *54*, 8396-8400.

45. Taylor, J. M.; Dekura, S.; Ikeda, R.; Kitagawa, H. *Chem. Mat.* **2015,** *27*, 2286-2289.
46. Gutov, O. V.; Molina, S.; Escudero-Adan, E. C.; Shafir, A. *Chem.-Eur. J.* **2016,** *22*, 13582-13587.
47. Liang, W. B.; Coghlan, C. J.; Ragon, F.; Rubio-Martinez, M.; D'Alessandro, D. M.; Babarao, R. *Dalton Trans.* **2016,** *45*, 4496-4500.
48. Cai, G. R.; Jiang, H. L. *Angew. Chem.-Int. Edit.* **2017,** *56*, 563-567.
49. DeStefano, M. R.; Islamoglu, T.; Hupp, J. T.; Farha, O. K. *Chem. Mat.* **2017,** *29*, 1357-1361.
50. Garibay, S. J.; Cohen, S. M. *Chem. Commun.* **2010,** *46*, 7700-7702.
51. Huang, Y. T.; Qin, W. P.; Li, Z.; Li, Y. W. *Dalton Trans.* **2012,** *41*, 9283-9285.
52. Lowell, S.; Shields, J. E.; Thomas, M. A.; Thommes, M. Mesopore Analysis. In *Characterization of Porous Solids and Powders: Surface Area, Pore Size and Density*, Lowell, S.; Shields, J. E.; Thomas, M. A.; Thommes, M., Eds. Springer Netherlands: Dordrecht, 2004; pp 101-128.
53. Sing, K. S. W.; Rouquerol, F.; Llewellyn, P.; Rouquerol, J. Ch. 9 - Assessment of Microporosity. In *Adsorption by Powders and Porous Solids (Second Edition)*, Rouquerol, J.; Rouquerol, F.; Llewellyn, P.; Maurin, G.; Sing, K. S. W., Eds. Academic Press: Oxford, 2014; pp 303-320.
54. van Beek, W.; Safonova, O. V.; Wiker, G.; Emerich, H. *Phase Transit.* **2011,** *84*, 726-732.
55. Knudsen, E. B.; Sorensen, H. O.; Wright, J. P.; Goret, G.; Kieffer, J. *J. Appl. Crystallogr.* **2013,** *46*, 537-539.
56. Petříček, V.; Dušek, M.; Palatinus, L. *Z. Kristallog.* **2014,** *229*, 345-352.
57. Ravel, B.; Newville, M. *J. Synchrot. Radiat.* **2005,** *12*, 537-541.
58. Momma, K.; Izumi, F. *J. Appl. Crystallogr.* **2011,** *44*, 1272-1276.
59. Trotter, J. *Acta Cryst.* **1960,** *13*, 732-736.
60. Derissen, J.; Timmermans, C.; Schoone, J. *Cryst. Struct. Commun.* **1979,** *8*, 533-536.
61. Kress, R. B.; Duesler, E. N.; Etter, M. C.; Paul, I. C.; Curtin, D. Y. *J. Am. Chem. Soc.* **1980,** *102*, 7709-7714.
62. Fitzgerald, L. J.; Gerkin, R. E. *Acta Crystallogr. Sect. C-Cryst. Struct. Commun.* **1993,** *49*, 1952-1958.
63. Jing, L.-H.; Qin, D.-B.; Mao, Z.-H.; Gu, S.-J.; Zhang, H.-X. *Acta Cryst. E* **2005,** *61*, o4365-o4366.
64. Borfecchia, E.; Gianolio, D.; Agostini, G.; Bordiga, S.; Lamberti, C. Characterization of MOFs. 2. Long and local range order structural determination of MOFs by combining EXAFS and diffraction techniques. In *Metal Organic Frameworks as Heterogeneous Catalysts*, Llabrés i Xamena, F. X.; Gascon, J., Eds. Royal Soc Chemistry: Cambridge, 2013; pp 143-208.
65. Barrett, E. P.; Joyner, L. G.; Halenda, P. P. *J. Am. Chem. Soc.* **1951,** *73*, 373-380.
66. Thommes, M.; Kaneko, K.; Neimark, A. V.; Olivier, J. P.; Rodriguez-Reinoso, F.; Rouquerol, J.; Sing, K. S. W. *Pure Appl. Chem.* **2015,** *87*, 1051-1069.
67. Brunauer, S.; Emmett, P. H.; Teller, E. *J. Am. Chem. Soc.* **1938,** *60*, 309-319.
68. Langmuir, I. *J. Am. Chem. Soc.* **1916,** *38*, 2221-2295.

For Table of Contents Use Only

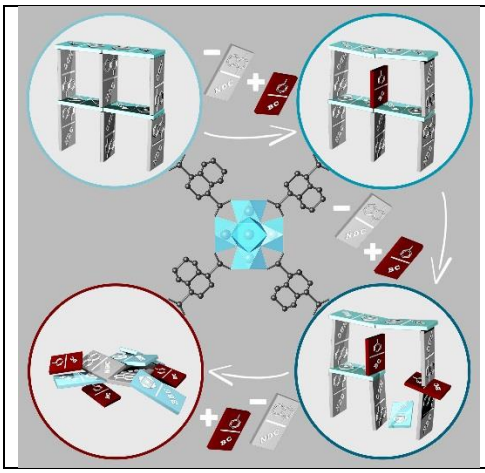

UiO-66-NDC MOF (NDC = 1,4-naphthalenedicarboxylic) has been synthesized and characterized using different fraction of benzene-carboxylic (BC) acid modulator vs. NDC to tune structural properties of the final product. Modulator increases both the crystal size and the surface area of the product, but reduces its thermal stability owing to insertion of defects: missing linkers and missing $Zr_6(OH)_4O_4$ clusters.